PERGAMON

Continental Shelf Research 20 (2000) 2067–2093

CONTINENTAL SHELF RESEARCH

The structure of the Eel River plume during floods

W. Rockwell Geyer[a,*], P. Hill[b], T. Milligan[c], P. Traykovski[a]

[a] *Applied Ocean Physics and Engineering Department, Woods Hole Oceanographic Institute, Woods Hole, MA, USA*

[b] *Department of Oceanography, Dalhousie University, Halifax, Nova Scotia, Canada*

[c] *Habitat Ecology Section, Bedford Institute of Oceanography, Dartmouth, Nova Scotia, Canada*

Abstract

Several large floods of the Eel River in northern California occurred during 1997 and 1998, with peak discharge ranging from 4000 to 12,000 $m^3 s^{-1}$. The flood conditions persisted for 1–3 days and were usually accompanied by strong winds from the southern quadrant. The structure of the river plume was strongly influenced by the wind-forcing conditions. During periods of strong southerly (downwelling favorable) winds, the plume was confined inside the 50-m isobath, within about 7 km of shore, with northward velocities of 0.5–1 $m s^{-1}$. Occasional northerly (upwelling favorable) winds arrested the northward motion of the plume and caused it to spread across the shelf. Sediment transport by the plume was confined to the inner shelf (water depths less than 50 m), during both southerly and northerly wind conditions. During southerly wind periods, fine, unaggregated sediment was rapidly transported northward to at least 30 km from the river mouth, but flocculated sediment was deposited within 1–10 km of the river mouth. During northerly (upwelling-favorable) winds, most of the sediment fell out within 5 km of the mouth, and negligible sediment was carried offshore, even though the low-salinity plume extended beyond the 60-m isobath. Although sediment deposition from the plume is confined to the inner shelf, the stratigraphy indicates that the principal flood deposits on the adjacent continental shelf occur in a patch between the 60- and 90-m isobath. Thus, the deposition on the inner shelf is ephemeral, and some mechanism other than plume transport delivers the sediment from the inner shelf to the mid-shelf.

Keywords: River plumes; Sediment transport; Eel River; Floods

*Corresponding author.

0278-4343/00/$ - see front matter
PII: S0278-4343(00)00063-7

1. Introduction

Milliman and Syvitski (1992) determined that a large fraction of the sediment entering the oceans from continents comes from small, high-relief drainage basins. The delivery of sediment from these rivers to the coastal ocean occurs in freshwater plumes, whose trajectories may strongly influence the ultimate fate of the sediment (Morehead and Syvitski, 1999). The dynamics and structure of plumes of small rivers differ considerably from those of large rivers, due to differences in the physical scales of the processes near the river mouth (Garvine, 1995) and relatively short duration of floods from small, high relief rivers compared to large river systems (Nash, 1994).

The short duration of flood events in small rivers may lead to a more important role of synoptic scale (1–5 day duration) meteorological forcing on the trajectory of the plume than in large river systems. Large rivers such as the Amazon or the Mississippi have freshet periods that extend over months, so the fate of the discharge plume depends on forcing conditions over seasonal time scales (Lentz and Limeburner, 1995; Geyer et al., 1996). Small and intermediate-size rivers with steep drainage basins exhibit markedly different behavior; freshet events can be extremely short-lived, occurring virtually on the same time scale as the meteorological events that supply the precipitation. Thus, the wind forcing during the brief period of high flow may determine the structure of the plume (Chao, 1988b) and the fate of the sediment discharged onto the continental shelf.

The transport of sediment in river plumes is controlled not only by the trajectory of the freshwater plume, but also by settling. Over the shallow, inner continental shelf, river plumes may remain in contact with the bottom boundary layer, whereas in deeper water, the plume separates from the bottom (Yankovsky and Chapman, 1997). After the plume has separated from the bottom boundary layer, sediment can no longer be maintained in the water column via resuspension, so a river plume will start to lose sediment as soon as it separates from the bottom boundary layer. The trajectory of sediment within the plume thus depends on the rate of settling, the plume thickness and plume velocity. The freshwater plume may be much more extensive than the sediment plume, particularly if the velocities in the plume are low, allowing the sediment to settle out before being carried far from the mouth.

A recent study of the Eel River in northern California provides an unprecedented set of observations of the structure of a plume emanating from a small, high-relief river during floods. The Eel River has one of the highest rates of sediment supply relative to area of any North American river (Brown and Ritter, 1971). The sediment load is dominated by brief, severe floods that occur during the winter months. During one flood in January, 1995, the Eel delivered an estimated 22 million tons of sediment to the coastal ocean (Wheatcroft et al., 1997). A distinct flood deposit of fine-grained sediment with a thickness of up to 10 cm and a length of 30 km was identified from sediment cores on the Eel River shelf between the 60- and 90-m isobaths. One possible explanation for the distribution of sediment on the shelf is the trajectory of the freshwater plume. However, lack of information about the shape and velocity of the Eel River plume and of settling velocity of sediment within it

made it difficult of assess whether the plume could have delivered the sediment directly to the flood deposit.

A field study was undertaken in the winters of 1996–1997 and 1997–1998 to determine the structure of the Eel River plume during floods, to quantify the transport of suspended sediment by the plume, and to assess its role in the formation of flood deposits. A large flood event occurred in January 1997, comparable in magnitude to the 1995 event. Several moderate events also occurred in the winter of 1998, due to the high rainfall associated with El Niño conditions. A combination of helicopter surveys and moorings provided measurements of salinity, temperature, suspended sediments and currents within the plume and the adjacent waters over the continental shelf. These observations provide the basis for an analysis of the dynamics of the plume and its freshwater and sediment transport during floods. The sediment transport calculations are then used to determine the role of the plume in the delivery of sediment to the continental margin and in the formation of sedimentary deposits on the continental shelf.

2. Methods

2.1. Site description

The Eel River enters the Pacific Ocean just north of Cape Mendicino, in Northern California (Fig. 1). Its discharge is generally low, but it usually has one or more large flows, lasting for several days, during the passage of winter storms (Brown and Ritter, 1971; Syvitski and Morehead, 1999). The Eel River has an unusually high sediment yield relative to its drainage area, due to the high relief and easily eroded bedrock (Brown and Ritter, 1971). The continental shelf adjacent to the river mouth is 10–15-km wide. During the winter months, the water column is weakly stratified, except during periods of high river flow (Largier et al., 1993).

The surficial sediment distribution on the shelf is dominated by sand at depths less than 50-m and by fine silt at greater depths (Borgeld et al., 1999). ^{210}Pb inventories indicate a depositional zone to the north of the mouth of the Eel, corresponding in location to the 1995 flood deposit, with accumulation rates as high as $0.8\,\mathrm{g\,cm^{-2}\,yr^{-1}}$ (Sommerfield & Nittrouer, 1999). Fine sediment accumulation also occurs on the continental slope at distances >50 km north of the mouth of the Eel, at rates of 0.2–$0.4\,\mathrm{g\,cm\,yr^{-1}}$ (Alexander and Simoneau, 1999).

2.2. Moored measurements

Moorings and tripods were deployed on the Eel Shelf in the winters of 1996–1997 and 1997–1998. In 1996–1997, moorings were also deployed at the 30- and 60-m isobath along the G-line (G-30 and G-60; see Fig. 1), for the period 16 December 1996–February 23 1997. The moorings consisted of surface buoys with Seacat temperature–salinity (T-S) sensors mounted to them at 0.5-m depth and S4 current

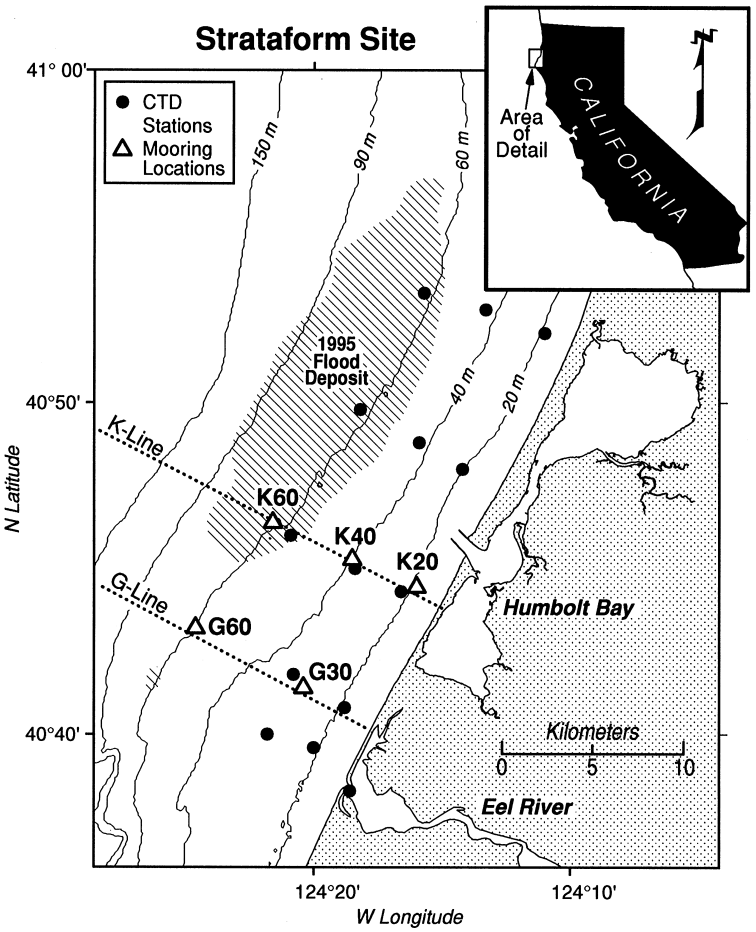

Fig. 1. Study area, showing the location of the 1995 flood deposit based on Wheatcroft et al. (1997). The sampling was all conducted north of the mouth of the Eel River, based on visual observations of the plume trajectory during helicopter flights. Moorings were occupied on the G-Line during 1997 and the K-Line during 1998.

meters at 2-m depth. The T-S sensors also included optical backscatterance sensors (OBSs) for estimating suspended sediment.

During the winter of 1997–1998, moorings were deployed at K-20, K-40 and K-60 (Fig. 1) from 21 November, 1997 to 25 March, 1998. Each mooring included Seacat T-S sensors at 0.5- and 4.5-m depths (all with OBS sensors) and S4 current meters at 2- and 6-m depths. A bottom tripod with a 1.2 mHz ADCP was deployed at K-20. It was buried by sediment on 21 January, but it was exhumed at the end of the study and provided velocity data from the beginning of the deployment to 21 January (see Traykovski et al. (this volume), for more details about the event leading to the burial of the tripod). The ADCP sampled at 0.5-m depth intervals through the water

column. Sampling periods of the instruments varied from 5 to 30 min. All of the data were averaged to 1 h.

2.3. Helicopter surveys

"Rapid Response" helicopter surveys were conducted with the assistance of the Coast Guard Group Humboldt Bay during major river discharge events. Helicopters were used rather than a research vessel because of the typically extreme sea conditions during floods. An instrument package was deployed using the helicopter's winch to obtain vertical profiles of water properties and to obtain discrete water samples. The package included an Ocean Sensors CTD and OBS, two 1.5–l Niskin bottles, and a floc camera for imaging particles. The Niskin bottles were automatically triggered at 1.5- and 10-m depths. The flights lasted for 1.5–2 h, and 3–14 stations were occupied, depending on weather conditions and other responsibilities of the flight crew. During the 1996–1997 observations, the instrument package did not reach the bottom, but during the 1997–1998 observations, the sensor package was lowered to the bottom at most stations (Fig. 1).

The CTD sampled at 2 Hz during the 1996–1997 observations and 5 Hz in 1998, corresponding to vertical resolution of 0.3- and 0.1-m, respectively. The water samples were transferred into 1-l Nalgene bottles onboard the helicopter and were filtered for total suspended solids using an 8 μm fiberglass filter. Disaggregated sediment size distributions were determined using a Coulter Counter (Milligan and Krank, 1991) and in situ floc size distributions were calculated by size analysis of photographs taken by the floc camera (Hill et al., this volume).

The OBS on the profiler was calibrated against the bottle data, aggregating all of the data from each year. There were no significant differences between the response curves for different cruises. For 1996–1997, the regression coefficient was $r^2 = 0.95$ ($n = 31$) for the calibration. For the 1997–1998 data, the calibration of the instrument was adjusted after the seventh survey to extend the range of measurements, so there were separate calibrations for the two settings. The regression coefficient for the first calibration was $r^2 = 0.81$ ($n = 43$) and the regression for the second set was $r^2 = 0.96$ ($n = 21$). The calibration of the moored OBS sensors was accomplished based on point comparisons with bottle samples during the helicopter surveys. The measurements were also compared to values from the surveys. There was evidence of fouling in both OBS records at K-60 and the deep sensor at K-40 during 1998, based on rapidly increasing backscatter at the ends of the timeseries that was uncorrelated with other hydrographic properties. Fouling did not appear to be a problem during the shorter deployment in 1996–1997, and there was no evidence of fouling of the instruments at K-20 or the surface instrument at K-40 during 1997–1998.

A total of seven surveys were performed in 1996–1997, nine in 1997–1998, and four in 1998–1999. This paper focusses on a major flood that occurred from 30 December 1996 to 3 January 1997, and a series of floods in January and February, 1998.

2.4. Other data

Wind and wave data were obtained from the NOAA buoy NDBC 46022, located at the 150-m isobath near the G-line, and NDBC 46030, located near Cape Mendicino, approximately 30-km south of the mouth of the Eel. Buoy 46022 data were used during 1997–1998, but the data were unavailable during early January, 1997, so the 46030 data were used for the 1996–1997 analysis. River discharge data were obtained by two USGS gauging stations: the Eel River at Scotia and the Van Duzen at Bridgeville, which together account for more than 90% of the flow of the Eel at the mouth.

3. Results

3.1. New-Year's flood, 1996–1997

The forcing conditions for the large 1997 event are shown in Fig. 2. This event had the highest discharge recorded since 1964 (Brown and Ritter, 1971), during which the largest recorded flood occurred. The high flow occurred over a 3-day period during which a major storm supplied high precipitation and strong southerly winds. Winds peaked at $20\,m\,s^{-1}$ on 31 January, close to the time that the river flow first exceeded $10{,}000\,m^3\,s^{-1}$. The southerly winds subsided to $10\,m\,s^{-1}$ for the next two days during the peak flow of the river, and on 3 January, the low-pressure system moved landward and the winds abruptly shifted to northerly. The along-shelf currents at 2-m depth at G-30 approximately tracked the winds, with the addition of a tidal oscillation of $\pm 30\,cm\,s^{-1}$. The surface salinity at G-30 indicates that the freshwater plume only briefly reached the mooring on 28 December, and it did not reappear until 3 January, following the wind reversal. Thus for most of the discharge event, the measured currents reflect conditions outside the river plume.

Analysis of the moored data for the whole deployment period at G-30 and G-60 indicates that the along-shelf currents are highly correlated across the shelf ($r = 0.84$ between the surface currents at the two locations). The along-shelf currents are also highly correlated with the winds (At G-60, near- surface, $r = 0.70$ at 9 h lag; at G-30, near-surface, $r = 0.65$, 4 h lag). These statistics indicate that the shift in along-shelf currents following the wind reversal on 3 January is typical of the along-shelf response during the winter months. Likewise the strong along-shelf currents during the peak discharge can be attributed mainly to the wind forcing.

Although the G-30 mooring was too far offshore to provide information about the plume during the flood, there were four helicopter surveys during the event (note times indicated by the triangles in Fig. 2) that document the structure of the plume. The surface salinity distribution (Fig. 3) indicates that the plume was narrower during the downwelling period (31 December and 2 January), even though this was the time of maximum outflow. Only after the winds reversed on 3 January did the plume begin to spread offshore. The measurements on 2 January included data in the nearshore part of the plume (along the 20-m isobath); these indicated surface

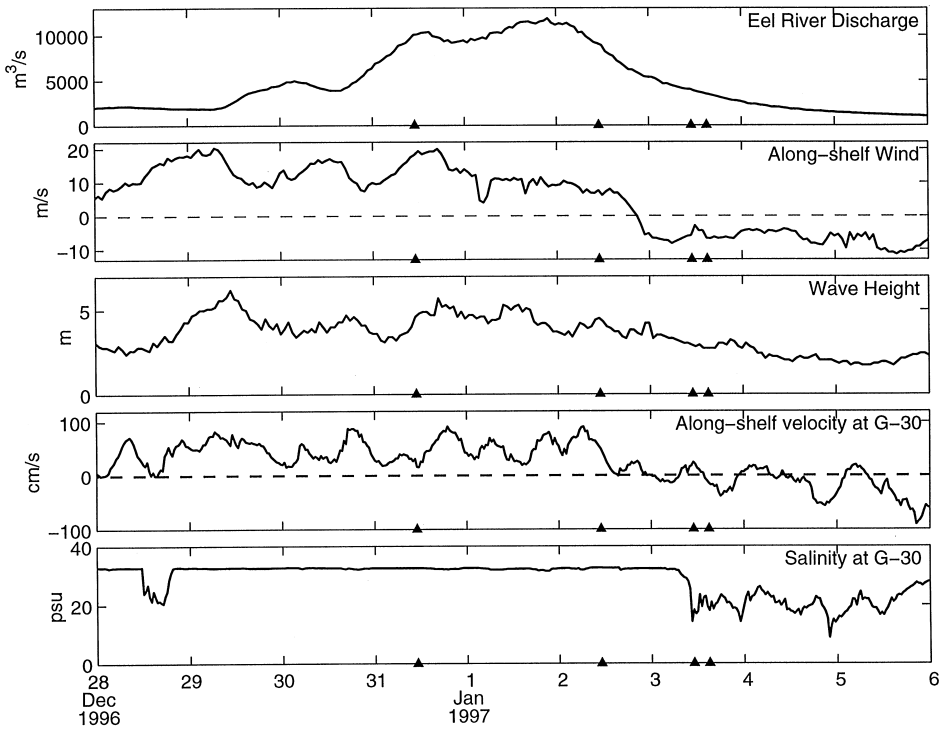

Fig. 2. Timeseries of forcing variables and conditions at the G-line during the large, 1997 flood. Top panel: Eel River discharge (measured at Scotia); second panel: along-shelf wind measured at NOAA buoy 46030 (near Cape Mendicino); third panel: wave height measured at buoy 46030; fourth panel: along-shelf velocity at G-30, 2 m below the water surface; bottom panel: salinity at g-30, 0.5 m below the water surface. Times of helicopter surveys are shown by triangles.

salinities of 15–20 psu compared to an ambient shelf salinity greater than 32. The vertical structure of the plume is indicated in cross-sections at the K-line (Fig. 3, lower panels). The plume was 6–7-m thick at the K-line during downwelling-favorable winds, and it thinned to 3 m as it extended offshore during the afternoon of 3 January, forced by upwelling-favorable winds.

The suspended sediment distribution (Fig. 4) closely resembled the salinity distribution during the first two surveys (high flow and downwelling condition), with concentrations of as much as $1500\,mg\,l^{-1}$ within the plume, and negligible sediment outside the plume. During the last two surveys (falling flow, upwelling-favorable winds), concentrations still reached $1000\,mg\,l^{-1}$ at the G-line (3–5-km north of the mouth), but the concentrations fell off sharply both in the offshore and along-shore directions within the plume. The vertical structure of the sediment distribution was similar to salinity during the first two surveys, with a strong concentration gradient at the base of the plume. In contrast, the concentration was relatively uniform with depth on the third survey and increased with depth on the fourth

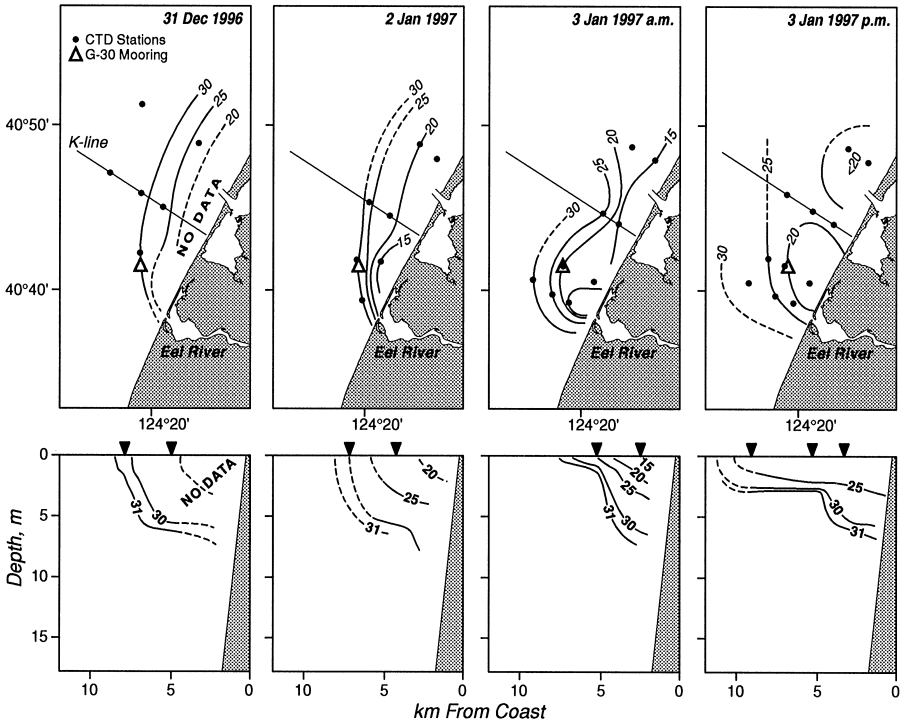

Fig. 3. Salinity distributions from helicopter surveys during the January 1997 flood. Upper panels: near-surface (1.5 m) salinity distributions; lower panel: cross-sections at the K-line. The seaward limit of the plume was estimated by visual observation from the helicopter.

survey. These observations indicate that the suspended sediment was behaving nearly conservatively within the plume during the high-flow, downwelling conditions, and that sediment was being lost to settling during the falling-flow, upwelling conditions.

A vertical section along the plume, following the 20-m isobath in the along-shelf direction (Fig. 5) demonstrates that the plume was confined to the near-surface waters. Near the mouth, the plume was only 3-m thick, and it increased to 6–8-m thickness by 18-km north. The plume spread more in the vertical on January 2 during southerly winds, suggesting mixing at the base of the plume, whereas the base of the plume remained intact on January 3 during weak northerly winds, suggesting the absense of mixing. Discrete suspended sediment measurements along this section indicate nearly conservative behavior of sediment within the plume on January 2, with high concentrations persisting to 18-km north. On January 3, the concentrations in the plume dropped by a factor of 4 at 11-km and by a factor of 50 at 18-km, indicating much more loss of sediment from the plume during the upwelling conditions. Concentrations beneath the plume increased between the mouth and 11-km, consistent with the raining out of sediment from the plume.

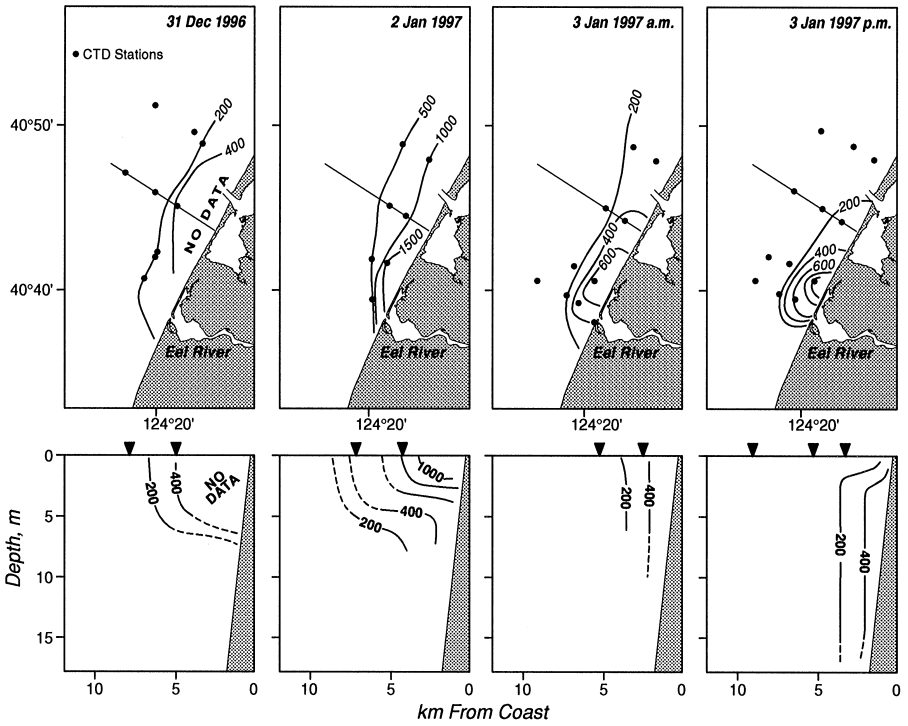

Fig. 4. Total suspended sediment distributions from helicopter surveys during the 1997 flood. Upper panels: near-surface (1.5 m) suspended solids, based on water samples; lower panel: cross-sections at the K-line, based on water samples and OBS profiles.

3.2. 1998 floods

The discharge peaks of the 1998 floods were approximately one third the amplitude of the large 1997 flood, but the multiple events provides a variety of forcing conditions (Fig. 6). Three events that occurred under distinctly different forcing conditions are shown by the dashed lines. The first (15 January 1998, labeled "slow") corresponds to a peak discharge during a wind reversal (i.e., northerly winds), the second (17 January, labeled "fast") to high flow with strong southerly winds, and the third (19 January, labeled "rough") to moderate southerly winds but extreme wave conditions. Currents measured at the K-line during this period show the wind-driven, along-shelf motions on which tidal currents are superimposed. The along-shelf currents were close to zero during the "slow" period; they were more than $50\,\mathrm{cm\,s^{-1}}$ along-coast during the "fast" period, and they were around $40\,\mathrm{cm\,s^{-1}}$ during the "rough" period. The salinity and turbidity do not consistently track the inputs from the river (Fig. 6), due to variations in cross-shelf structure of the plume during different wind conditions. For example, large peaks in turbidity at K-20 occurred during several of the large discharge events, but they were absent

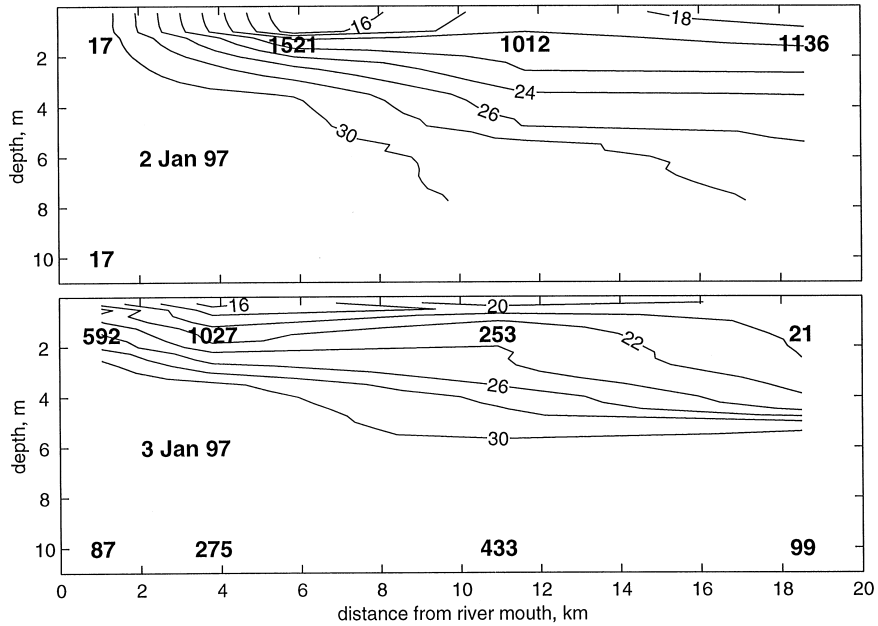

Fig. 5. Along-shelf vertical sections at the 20-m isobath of salinity on January 2 1997 (near the peak of the flood) and January 3 1997 (after the wind had shifted to northerly). Bold numbers are suspended sediment measurements from water samples. (Note that some 10-m samples were not obtained during the January 2 survey).

during the events that occurred during upwelling-favorable winds (e.g., January 15 and 26).

The variability of the plume structure as a function of forcing conditions is revealed in cross-sections of salinity and suspended sediment (Fig. 7). The salinity plume extended farthest across the shelf during upwelling-favorable (or "slow") conditions, but the suspended sediment distribution was most limited during these times. The suspended sediment and salinity had similar spatial structure during downwelling-favorable winds, i.e. "fast" conditions, and the high concentration of suspended sediment extended further offshore than during "slow" conditions. This difference is explained by the shorter transit time within the more rapidly advecting plume, which provided less time for settling to occur. A notable feature of the sediment distribution in all cases was a bottom turbid layer; this layer was much thicker and had much higher concentrations during the "rough" conditions. The concentration could not be resolved by the vertical profiles, because it exceeded the gain setting of the OBS ($C > 450\,mg\,l^{-1}$).

There is evidence that the concentrations were much higher than 450 mg/l in this near-bottom zone during the "rough" conditions. The apparent salinity measured by the CTD dropped by as much as 1 psu near the bottom at K-20 (Fig. 8), which may be explained by the reduced conductivity of high concentrations of suspended

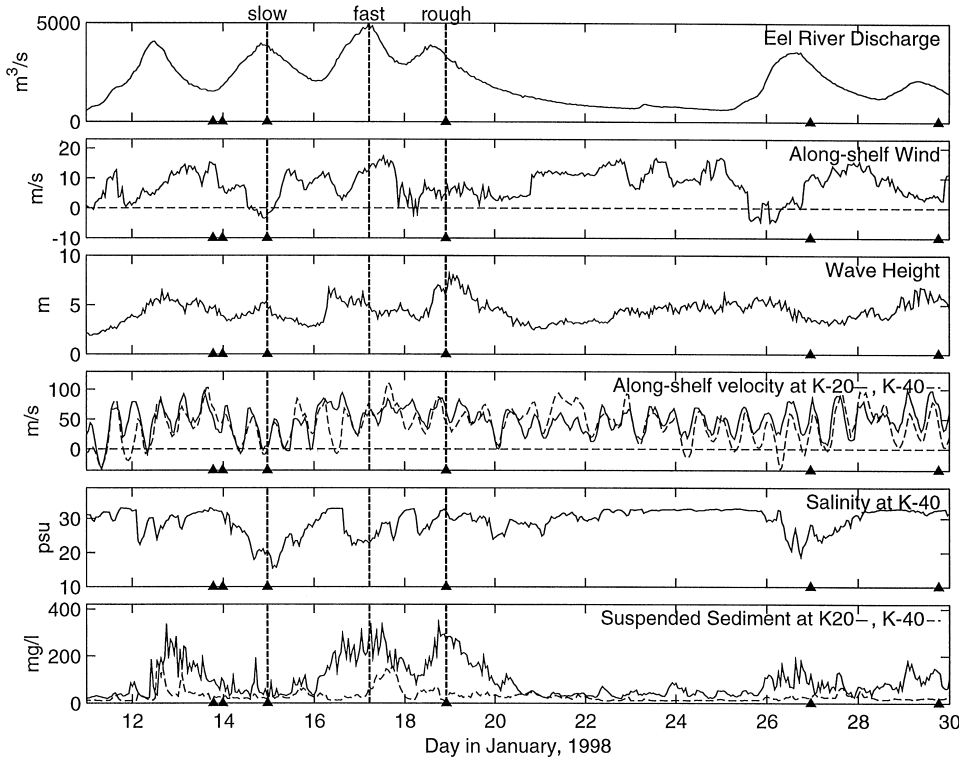

Fig. 6. Timeseries of forcing variables and conditions at the K-line during a series of moderate discharge events in 1998. Top panel: Eel River discharge; second panel: along-shelf wind measured at NOAA buoy 46022 (near the mouth of the Eel); third panel: wave height measured at buoy 46022; fourth panel: along-shelf velocity at K-20 (solid) and K-40 (dashed), 2-m below the water surface; fifth panel: salinity at K-40, 0.5 m below the water surface; bottom panel: suspended sediment at K-20 (solid) and K-40 (dashed), 0.5 m below the surface. (The salinity sensor at K-20 was clogged and did not provide useful data during this period). The three time periods labeled "slow", "fast" and "rough" correspond to cross-sections in Fig. 7. Times of helicopter surveys are shown by triangles.

sediment (Kineke and Sternberg, 1992). Calculations by Traykovski et al. (this volume) indicate that such a decrease in apparent salinity would require concentrations in the fluid mud range ($50–100 \times 10^3\,mg\,l^{-1}$). In addition, the output of the OBS decreased abruptly within the turbid layer (Fig. 8). Kineke and Sternberg (1992) showed that at fluid mud concentrations, the output of the OBS actually decreases. For the gain setting of this instrument this effect would not be observed until the concentrations reached approximately $50 \times 10^3\,mg\,l^{-1}$. Additional, perhaps more direct, evidence comes from the moored ADCP data at this location. Approximately 5 h after the helicopter CTD observations of January 19, the ADCP was buried under nearly 1-m of sediment (see Traykovski et al. (this volume) for more details).

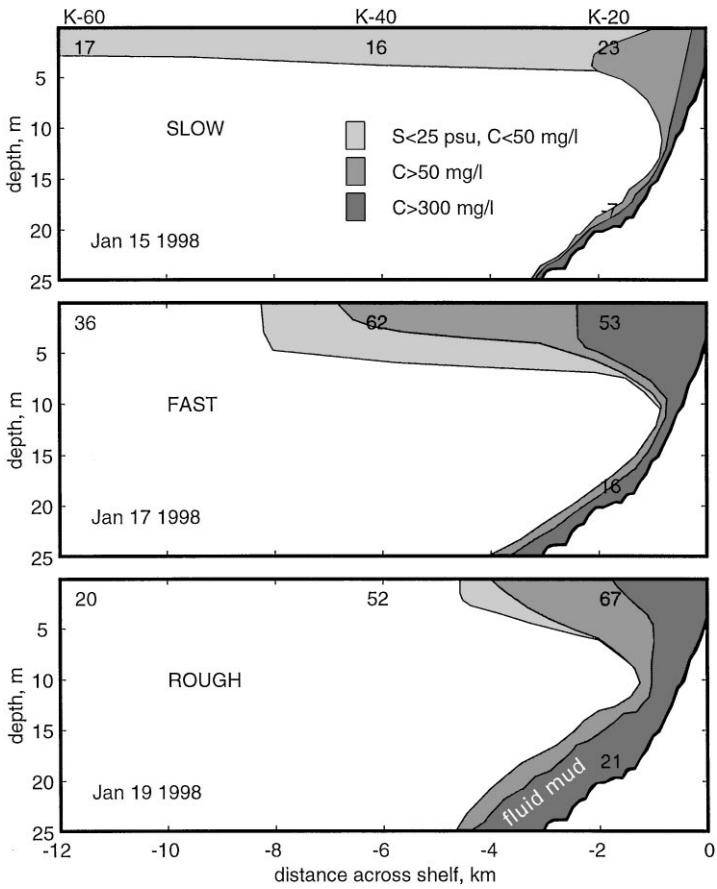

Fig. 7. Cross-sections of suspended sediment and salinity structure of the plume at the K-line during three time-intervals indicated on Fig. 6. The light shading correspond to low-salinity plume water with suspended sediment concentrations $C < 50\,mg\,l^{-1}$. The darker shading indicates higher suspended sediment concentrations. Numbers indicate along-shelf velocities in cm s^{-1}. The upper panel corresponds to "slow" conditions, when northerly winds slowed down the plume and caused offshore advection of fresh water. The middle panel corresponds to "fast" conditions, when strong southerly winds caused rapid northward advection. The bottom panel corresponds to "rough" conditions, when wave resuspension produced a thick, high-concentration turbid layer with evidence of fluid mud. The plume structure landward of K-20 is speculative; there were no observations in that region.

The salinity and suspended sediment profiles can be compared to the velocity structure at K-20 for the helicopter surveys prior to January 20, before the ADCP was buried (Fig. 8). Both salinity and velocity showed strong vertical gradients through the plume (down to 6–10-m depth), and they were uniform beneath the plume. There was no evidence of a surface mixed layer — the salinity gradient extended to within 1-m of the surface, even on January 14 when the wind velocities reached $10\,m\,s^{-1}$. The suspended sediment profiles indicate approximately linear

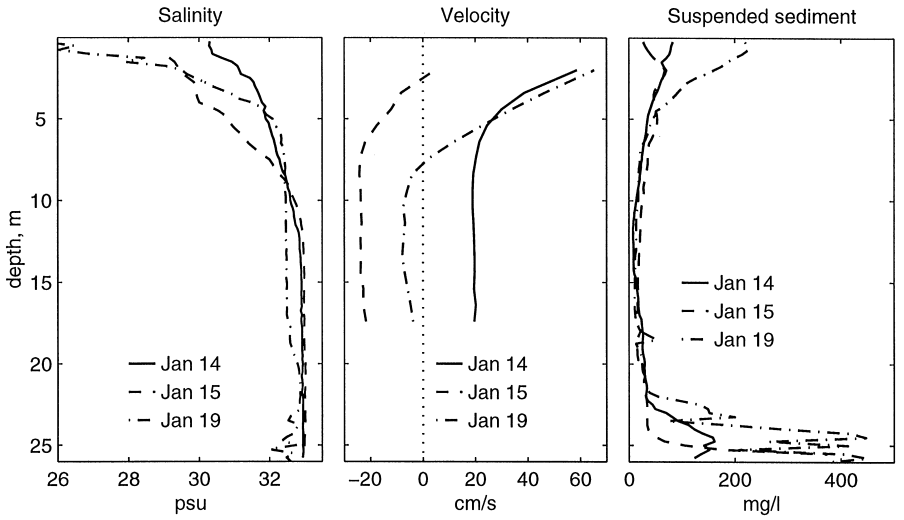

Fig. 8. Vertical profiles of salinity, velocity, and suspended sediment at K-20 during three helicopter surveys in 1998. The velocity data were obtained from the bottom-mounted ADCP at the 20-m isobath, whereas the salinity and suspended sediment data were obtained during helicopter surveys at the 26-m isobath. The near-bottom sediment concentrations on January 19 are believed to be much higher than indicated on the figure, as discussed in the text.

variation in concentration in the plume, except for January 15 in which the near-surface concentration decreased, most likely due to settling of sediment. A bottom turbid layer was evident in all of the profiles, with the highest near-bed concentrations occuring on January 19. The downward spikes in the profile on January 19 are evidence for extremely high concentrations, as noted above. There were large variations in barotropic (or vertically averaged) velocity, due both to tides and wind-driven motions, but the shear was more closely tied to the salinity structure (see discussion).

4. Analysis and discussion

4.1. Dynamics of the plume and shelf region

4.1.1. Tides

The current meter observations indicate that the tides are mainly barotropic, with semidiurnal velocity amplitudes of around $15\,\mathrm{cm\,s^{-1}}$ and diurnal amplitudes around $10\,\mathrm{cm\,s^{-1}}$. The principal axes are oriented in the along-coast direction, and ellipticity is small near the coast but it increases offshore. When the semi-diurnal and diurnal components were in phase, variations in along-shelf velocity of as much as $50\,\mathrm{cm\,s^{-1}}$ occurred as a result of the tides, representing a significant perturbation on the motion of the plume. Tidal exchange through Humboldt Bay is also likely to affect

the plume, with an offshore-directed momentum source during ebb tides that is comparable to the momentum of the river during peak discharge conditions (roughly 10,000 $m^3 s^{-1}$ during large ebbs). The tidal jet should distort the plume and provide energy for mixing and sediment resuspension. Some of the profiles indicated significantly deeper penetration of brackish water to the north of the mouth of Humboldt Bay relative to the profiles further south, suggesting that mixing associated with the inlet may affect the plume. Because of this potential effect, the analysis of plume transport processes was focussed to the south of the inlet.

4.1.2. Wind-driven motions

The along-shelf winds provide a major source of variability of the along-shelf currents. Based on linear regression between the moored velocity measurements at the K-line and the NOAA Buoy 46022 winds in 1998, the near-surface, (2-m depth), along-shelf currents have a response of approximately 1 m s^{-1} per Pa of along-shelf wind stress. The strength of the response decreases to 20–40% of this value beneath the plume. The currents lag the winds by roughly 6 h. Approximately 50% of the low-frequency variance at the surface is explained by the wind stress, based on analysis of the 1998 data at K-20 and K-40. There is also evidence of an Ekman response of the cross-shelf currents to along-shelf wind stress, although it is only 10% of the strength of the along-shelf response. The response to cross-shelf winds was not significant.

The nature and magnitude of the response to winds is consistent with other continental shelf observations and theory (Allen, 1980, Lentz and Winant, 1986, Lentz et al., 1999). Landward Ekman transport in the surface layer during downwelling-favorable winds causes a set-up of the sea surface against the coast and deepening of the pycnocline, which drives a geostrophic flow that weakens with depth due to the baroclinic gradient associated with the cross-shore salinity gradient. During upwelling winds, essentially the reverse process occurs, except that the cross-shelf baroclinic gradient is weakened as the plume advects offshore.

The winds are particularly important to the motion of the plume, because the along-shelf winds are significantly correlated with river discharge, with northward directed wind stress tending to occur during high discharge conditions. Based on the 1998 data, the peak wind stress leads the discharge by 1.5 days (correlation coefficient $r = 0.46$, degrees of freedom $n > 20$), but there is still significant correlation at 0 lag ($r = 0.24$, $n > 20$). This correlation results from the association of large precipitation events with low pressure systems, which produce strong southerly winds along the coast. In 1998, the average northward wind stress during discharge events ($Q > 800\ m^3 s^{-1}$) was 0.15 Pa, which yields an average of 15 cm s^{-1} of wind-induced, along-shelf flow at the surface, based on the above regression analysis. Non-event periods ($Q < 800\ m^3 s^{-1}$) had an average wind stress of 0.03 Pa, which is not significantly different from zero.

The wind stress strongly affects the cross-shelf structure of the river plume, consistent with previous studies (Chao, 1988b, Fong, 1998). Southerly (downwelling-favorable) winds confine the plume to the inner shelf, whereas the occasional northerly (upwelling-favorable) wind events spread the plume across the shelf. Wind

stress also appears to affect mixing within the plume, as inferred above in context with spreading at the base of the plume (Fig. 5). Note, however, that even with gale-force winds (e.g., Jan. 14, 1998; Fig. 6) the plume remained stratified to within 1-m of the water surface, indicating the strong stabilizing tendency of the buoyancy flux. Nor was there ever adequate stress for the resuspended sediment in the bottom boundary layer to affect the turbidity within the plume.

4.1.3. Riverine forcing

The freshwater inflow provides a direct input of momentum as well as a large buoyancy source, both of which contribute to the motion over the shelf. Visual observations from the helicopters as well as aerial photos indicate that over the last 20 years, the Eel River has been deflected northward by a vegetated sand-spit, so that it enters the ocean at an angle of about 20° to the along-shelf direction. Garvine (1982) showed that such an oblique angle of entry will produce a narrow, swift plume that remains attached to the coast. The velocity at the mouth could not be estimated precisely, but it could be estimated from transport considerations. During the peak of the flood in 1997, the discharge was $12{,}000\,\mathrm{m^3\,s^{-1}}$, the width at the mouth was approximately 1-km (in the direction normal to the flow), and the depth was estimated at 4–6 m (based on one CTD cast taken in the river mouth on January 3, 1997). This yields a peak outflow velocity of $2–3\,\mathrm{m\,s^{-1}}$. Some fraction of this momentum input would have been lost to bottom friction within the surf zone and inner shelf, but even half of the initial velocity would still represent a major component of the momentum input for the plume.

The buoyancy forcing can be estimated from the baroclinic pressure anomaly associated with the freshwater plume

$$P_f = g \int_{-h}^{0} (\rho_0 - \rho(z))\, \mathrm{d}z, \tag{1}$$

where ρ_0 is the ambient density, $\rho(z)$ is the vertically varying density due to dilution with fresh water, and h is the water depth. The largest observed value of p_f was 360 Pa (on January 2, 1997 at G-20) which is equivalent to 3.7 cm of sea-level displacement. Based on Bernoulli's equation, it has the same dynamic pressure as a velocity anomaly of $85\,\mathrm{cm\,s^{-1}}$. This indicates that the momentum flux from the river exceeds the buoyancy forcing, or, equivalently, that the internal Froude number near the mouth exceeds 1 (Armi, 1986). The main implication of this supercritical flow condition is that the dynamics in the vicinity of the mouth are strongly influenced by the momentum input from the river (Garvine, 1995). The spatial scale of this influence is defined by the inertial radius $L_i = u_f/f$, where u_f is a representative velocity within the plume and f is the Coriolis acceleration. This scale was on the order of 10-km during floods, indicating that inertial effects were important approximately as far as the K-line. The inertia of the outflow often produces a bulge in the plume adjacent to the mouth of a river with a scale close to the inertial radius (Chao and Boicourt, 1986); however the angle of the mouth of the Eel greatly reduces the offshore extent of the bulge (Garvine, 1982). The bulge evident during

upwelling conditions (Fig. 3, third panel) was not due to inertia, but rather to convergence of freshwater flux (see discussion below).

The near-surface, alongshore currents at the K-line were all significantly correlated with river discharge, with the highest correlation ($r = 0.65$, $n = 9$) occurring at K-20. The response to river discharge was bimodal, with weak alongshore flow in the absence of freshwater flow and strong northward flow during discharge events. This tendency is shown in Fig. 9, based on the ADCP data at K-20 in 1998. The near-surface velocity averaged over times of significant river discharge ($Q > 800\,m^3\,s^{-1}$) was nearly $50\,cm\,s^{-1}$, compared with around $10\,cm\,s^{-1}$ during low flow conditions. Part of the augmented flow (roughly $15\,cm\,s^{-1}$) is explained by the linear correlation of winds with discharge (as noted above). The response of the surface waters to winds is probably stronger when the plume is present, due to the suppression of turbulence by stratification (Kudrayavtsev and Soloviev, 1990). The direct forcing by the momentum of the river, as well as the buoyancy forcing, were certainly important contributors to the rapid northward motion of the plume, but their contributions relative to wind-forcing could not be quantified based on these observations.

The cross-shelf density gradient was in approximate geostrophic balance with the along-shelf shear within the plume, although there was considerable variability due to winds and tides that perturbed the balance. Thus, although the inertial terms were apparently significant in the along-plume momentum balance (based on the large

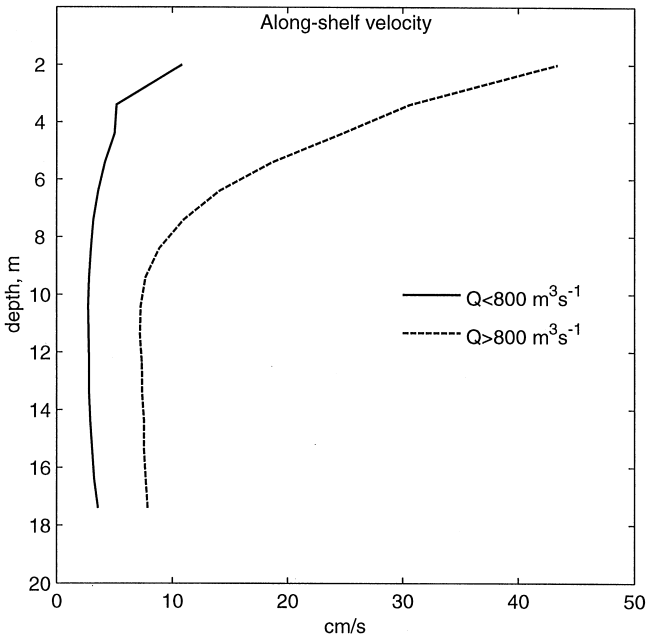

Fig. 9. Vertical profiles of velocity obtained at K-20 during 1998 for periods of low discharge ($Q < 800\,m^3\,s^{-1}$) and high discharge ($Q > 800\,m^3\,s^{-1}$).

Froude number at the mouth), the relatively straight trajectory of the plume produced only a minor contribution of inertia to the cross-plume balance, leading to a semi-geostrophic regime typical of large river plumes (Garvine, 1995).

The observed freshwater transport within the plume is comparable to model results (Chao, 1988a) and observations (Rennie et al., 1999) of the plume from Chesapeake Bay, which has comparable transport to the Eel River plume during floods. The lowest mode internal wave speed within the plume was estimated at 40–55 cm s^{-1} based on the helicopter CTD profiles; thus the Froude number within the plume was close to 1 (in constrast to the Froude number at the mouth, which significantly exceeded 1). The Froude number was significantly higher those found in the model studies of Chao (1988a), in which the values ranged from 0.1 to 0.5. This comparison indicates stronger forcing conditions for the Eel River plume, both due to wind forcing and the momentum input at the mouth.

Several other plume parameters help characterize this plume for comparison with other regimes. The "mouth" Kelvin number (Garvine, 1987) is defined by $K_m = L_m/L_D$, where $L_m = 2$ km is the width at the mouth and the deformation radius

$$L_D = (g'h)^{1/2}/f = 5 \text{ km}$$

(where $g' = \Delta\rho/\rho$ is the buoyancy anomaly of the plume, $h \approx 6$ m is the thickness of the plume, and $f = 0.9 \times 10^{-4}$ s^{-1} is the Coriolis parameter). Thus $K_m = 0.4$, which indicates that inertial effects at the mouth are important relative to the earth's rotation (Garvine, 1987). The "plume" Kelvin number $K_P = L_P/L_D$, where L_P is the plume width (Garvine, 1995) provides an indication of the overall importance of rotation within the plume. The plume width $L_P \approx 6$–8 km, indicating $K_P \approx 1$. This puts the Eel River plume into the transition between advection-dominated and rotation-dominated plumes.

Yankovsky and Chapman (1997) define a plume "lift-off" depth $h_b = (2Q_p f/g')^{1/2}$ where Q_P is the total transport of brackish water in the plume. At the time of maximum river flow, the freshwater transport was about 10^4 m^3 s^{-1}, but mixing with salt water increased the total transport Q_P by a factor of 4–5. The resulting lift-off depth $h_b \approx 13$ m for the maximum flow conditions. This calculation indicates, as is observed, that the plume should be detached from the bottom. The observed plume depth was roughly half of the calculated h_b, which is probably due to the along-shelf forcing of the plume by the plume by winds and barotropic currents, in contrast to the Yankovsky and Chapman theory in which baroclinic forcing is the only ingredient.

4.2. Freshwater transport in the plume

The freshwater balance within the plume was used to estimate the residence time of water within the plume and the advection speed of the plume. The calculation provides a characterization of the variability of the plume structure and provides important information for quantifying the sediment transport in the plume. The input of freshwater into the plume Q_f was based on the USGS gauging station data. The local "freshwater thickness" within the plume was

estimated by the integral

$$h_f = \frac{1}{s_0}\int_{-h}^{0}(s_0 - s)\,\mathrm{d}z \tag{2}$$

where s_0 is the ambient salinity (taken as the maximum salinity in a particular survey), and s is the depth-varying salinity in the plume. This quantity can be regarded as the thickness of the plume if it were "unmixed" with ambient water. The total freshwater content V_f was estimated by a trapezoidal estimate of the spatial integral of h_f for the stations south of and including the K-line from the hydrographic data. This estimate was crude, due to the small number of stations, but it provides an indication of the magnitude and variability of the freshwater content. Limiting the spatial integral to the southern portion of the plume reduced the variability associated with the tidal exchange of Humboldt Bay and provided a means of estimating the freshwater transport past the K-line. The residence time within this portion of the plume was estimated by V_f/Q_f.. The effective plume advection speed u_f was calculated in two different ways. During the first two surveys, the short residence times and similar plume structure suggested that the salt content was relatively steady relative to the flux, so the freshwater flux at the K-line was assumed to balance the freshwater input. Thus,

$$Q_f = u_f \int_0^{Lx} h_f\,\mathrm{d}x \tag{3}$$

provides a means of estimating the effective plume advection speed, where L_x is the width of the plume at the K-line and h_f is the freshwater thickness along the K-line. The plume width could only be estimated crudely, due to the finite spacing of the stations. During the last two surveys of 1997, the steady-state approximation was not valid due to varying freshwater content in the plume. For these cases, the change in freshwater content within the plume was subtracted from the freshwater input to calculate the flux at the K-line:

$$Q_f - \frac{\partial V_f}{\partial t} = u_f \int_0^{Lx} h_f\,\mathrm{d}x. \tag{4}$$

The average freshwater thickness was around 1-m during the 1996–1997 flood, and it averaged 0.6-m during the 1998 observations (Table 1). The volume of the plume, calculated between the mouth and the K-line, did not vary consistently with freshwater input, reflecting the variability of residence time of fresh water in the plume. The shortest residence time was 2.3 h during the strong wind forcing of the first survey. The longest residence time of 12 h occurred during the wind reversal on 3 January 1997. The effective plume speed u_f reached $1.3\,\mathrm{m\,s^{-1}}$ during the first survey and actually reversed on January 3. During the 1998 observations, there was less variability in residence time, although there was considerable variability in plume speed, due mostly to variations in winds. The relative velocity (Δu) between the plume and the underlying water showed similar dependence on winds. During the highest winds on December 31 1996, the plume was travelling nearly $1\,\mathrm{m\,s^{-1}}$ faster than the underlying water.

Table 1
Freshwater transport calculations[a]

	Q_f ($m^3 s^{-1}$)	v_{wind} ($m^3 s^{-1}$)	h_f (m)	L_x (km)	V_f (10^8 m^3)	T_r (h)	u_f ($m s^{-1}$)	u_a ($m s^{-1}$)	Δu ($m s^{-1}$)
31 Dec 1996	10,000	19	1.1	5	0.9	2.3	1.3[b]	0.22	0.9
2 Jan 1997	9 000	8	1.3	5	1.0	3.1	0.9[b]	0.40	0.5
3 Jan 1997 a.m.	3 500	−6	0.8	8	0.9	7.3	−0.2[c]	0.12	−0.1
3 Jan 1997 p.m.	3 000	−7	0.9	10	1.3	12.0	−0.1[c]	−0.12	0.0
14 Jan 1998	1 800	7	0.4	5	0.3	4.6	0.5[d]	0.0	0.5
15 Jan 1998	3 800	−3	0.6	10	0.9	6.6	0.1[d]	−0.2	0.3
27 Jan 1998	3 000	11	0.8	5	0.7	6.5	0.2[d]	−0.1	0.3
30 Jan 1998	1 800	4	0.4	5	0.3	4.6	0.8[d]	0.5	0.3
6 Feb 1998	2 500	13	0.7	5	0.6	6.7	0.6[d]	0.3	0.3
8 Feb 1998	3 700	5	0.5	10	0.8	6.0	0.5[d]	0.1	0.3

[a] Q_f is river discharge at the time of the survey, v_{wind} is the along-coast wind velocity, h_f is the average freshwater thickness in the plume, L_x is the average offshore extent of the plume, V_f is the integrated freshwater content of the plume, T_r is the plume residence time (between the mouth and the K-line, 12 km north of the mouth), u_f is the estimated velocity in the plume, u_a is the ambient velocity (from the G-30 near-surface current meter in 1997; from K-20 current meter at 6-m depth in 1998) , and Δu is the velocity difference between the plume and ambient flow.

[b] u_f based on steady freshwater balance.

[c] u_f based on unsteady freshwater balance.

[d] u_f estimated by direct velocity measurements at 2-m depth at K-20 and K-40.

4.3. Sediment transport and trapping

The observations from 1997 and 1998 were used to estimate the sediment transport by the plume and the delivery of sediment to different regions of the continental shelf. This was accomplished by calculating the amount of sediment discharging from the river and the amount transported by the plume past the K-line. These two flux estimates effectively define two regions of sediment delivery, divided in the north-south direction by the K-line. The offshore extent of the plume transport was defined by the observed sediment distribution in the plume. This calculation only considers the transport by the plume, and does not address the transport in the bottom boundary layer, which may have redistributed the sediment prior to its accumulation in flood deposits. The 1998 observations provide more comprehensive estimates of the sediment transport during floods than the 1996–1997 observations, however the magnitude of the 1996–1997 flood makes it worthwhile to attempt a sediment balance for that event, even if it has large uncertainty.

4.3.1. Sediment discharge from the river

The estimates of sediment discharge from the river were based on historical data as well as direct measurements at the mouth. Based on combined measurements of flow and concentration at Scotia between 1960 and 1980, Syvitski and Morehead (1999)

obtained a statistical relationship for the discharge dependence of concentration

$$C = \alpha Q^{\beta}, \tag{5}$$

where $\alpha = 0.347$ and $\beta = 1.139$, where C is in units of $\mathrm{mg\,l^{-1}}$ and Q in $\mathrm{m^3 s^{-1}}$ (Fig. 10). A similar regression was reported by Wheatcroft et al. (1997).

In addition to these historic data, suspended sediment samples at the mouth were obtained on eight occasions during floods in 1997 and 1998. The samples were obtained at 1.5-m depth, and the river depth at that location was typically 4-m, based on the depth reached by the profiler. The suspended sediment in these samples was made up entirely of material finer than sand, whereas the historical measurements at Scotia indicated approximately 25% sand. It was thus assumed that the sand did not enter the plume, and the historic data were adjusted downward by 25% in Fig. 10 for comparison with the river-mouth observations. The new observations fall within the scatter of the historic data, although they consistently lie below the regression line. Analysis of the interannual variability of the historic data indicates a decreasing trend in sediment yield between 1964 and 1980, which is consistent with the lower values of the recent observations.

Estimates of concentration at the mouth were obtained by using the slope β from Syvitski and Morehead (1999), but applying a range of values of α to encompass the recent observations. The upper value of α is the same as Syvitski and Morehead's, and the lower value is 0.14. These two estimates provide an approximate range of uncertainty of the concentration during the flood events.

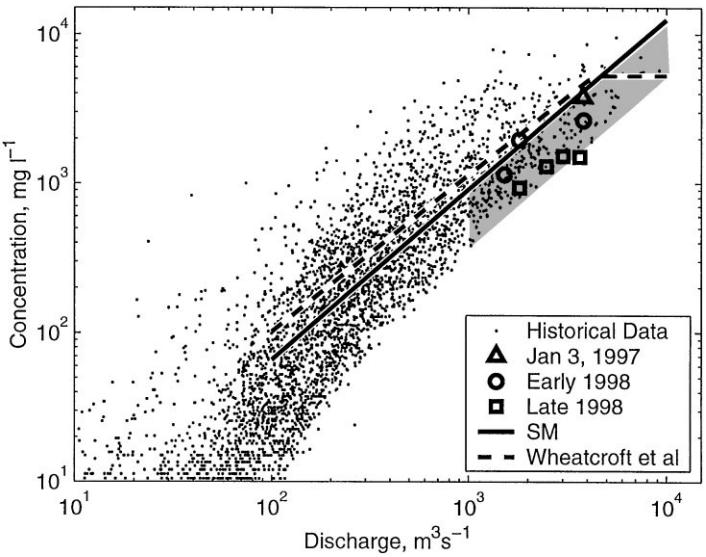

Fig. 10. Sediment concentration as a function of river discharge for historic data (small open circles) and the recent observations (large symbols). Wheatcroft et al. (1997) and Syvitski and Morehead (1999) (SM) rating curves are indicated. The shaded zone indicates the range of uncertainty of the rating curve for this analysis.

4.3.2. Plume sediment transport past the K-line

The sediment transport past the K-line was estimated in two ways: by direct flux estimates using velocity and concentration timeseries data (available only in 1998) and by an indirect method using the helicopter observations of salinity and suspended sediment (for both 1997 and 1998). For the 1998 observations, the concentration and velocity measurements in the near-surface waters at K-20, K-40 and K-60 were assumed to be representative of 4-km wide, 7-m deep segments of the plume, and the sediment flux was obtained by summing the contributions from each mooring. The flux beneath the plume and above the bottom boundary layer was not resolved by the moored instruments, although its contribution could be estimated based on the ADCP-derived velocity profiles and vertical profiles of sediment concentration during the helicopter surveys.

The indirect method was based on the assumption that the freshwater flux at the K-line equaled the river outflow. This is reasonable for the days during downwelling-favorable winds. The fluxes were assumed to be near zero (or southward) during upwelling-favorable conditions. Based on freshwater conservation, the volume flux in the plume could be estimated as

$$Q_p = \frac{s_0}{s_0 - s_p} Q_f, \tag{6}$$

where s_0 is the salinity beneath the plume and s_p is the salinity in the plume. The sediment flux is then

$$Q_{sed} = C_p Q_p = \frac{s_0}{s_0 - s_p} C_p Q_f, \tag{7}$$

where Q_{sed} is the flux of sediment and C_p is the sediment concentration in the plume. In the absence of settling, Q_{sed} would be invariant following water parcels within the plume as they mixed with seawater, but settling causes the concentration to deviate from a conservative mixing line and for the flux to decrease.

A comparison of the flux at the river mouth (based on the Eq. (5)) with the flux at the K-line is shown in Fig. 11, including the direct (solid lines) and indirect (circles) methods of calculation. The minor differences between the direct and indirect estimates probably relate to temporal and spatial variability of the freshwater and sediment flux. The large peaks in flux at the river mouth are associated with the major discharge events. The estimated flux at the K-line is significantly smaller than the sediment flux from the river, indicating that much of the sediment fell out of the plume before reaching the K-line. The greatest sediment losses occurred during times of high discharge and weak or upwelling-favorable winds (e.g., January 15). The smallest losses occurred during strong southerly winds (e.g., January 17). Integrated over the period from January 10 to February 10, the river delivered 5–12 million tons (based on the range of rating curve estimates), and the estimated transport in the plume past the K-line was 3 million tons. Thus, 25–60% of the sediment was exported past the K-line in the plume.

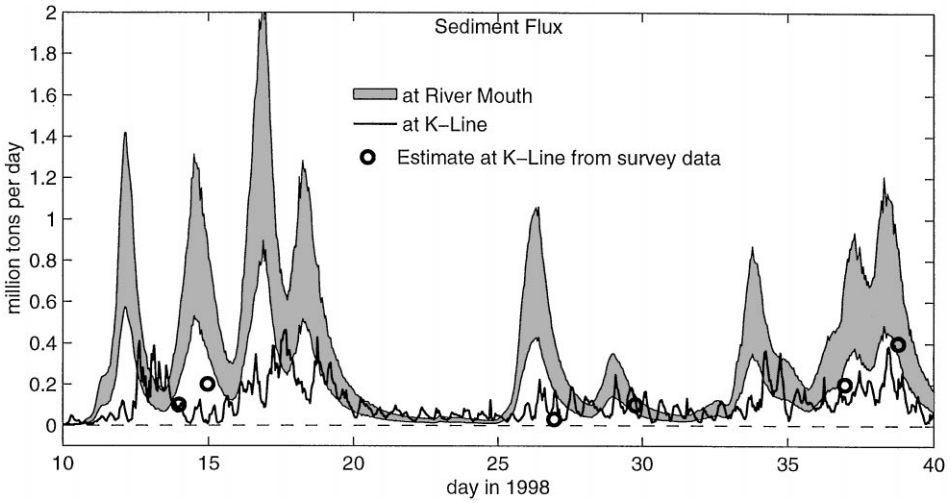

Fig. 11. Estimated sediment flux during 1998 at the river mouth (shading) and at the K-line (solid line). Estimates at the K-line from helicopter survey data are indicated by circles. The upper bound on the rivermouth flux estimate is based on Syvitski and Morehead (1999) and the lower bound uses a value $\alpha = 0.4$ in Eq. 5. The difference between the flux at the river mouth and the flux at the K-line is an estimate of the sediment that settled out of the plume to the south of the K-line.

These flux calculations only included the contributions of the plume to sediment transport, neglecting the rest of the water column. An approximate estimate of the contributions of sub-plume transport to the total flux was obtained by combining the ADCP velocity data and the helicopter survey data of sediment concentration (e.g., Fig. 8). The concentrations between the plume and the bottom boundary layer were generally low, as was the along-shelf velocity below the plume. As a consequence, the estimated flux in this intermediate zone was found to be roughly 10% of the flux in the plume. The concentrations in the bottom boundary layer could reach higher levels than the plume, so the transport in the bottom boundary layer could not be neglected. However, there were not adequate velocity or suspended sediment measurements in the bottom boundary layer to quantify the flux. A comparison of the fluxes in the plume and the overall distribution of flood sedimentation suggests that indeed, the bottom boundary layer transport is a major component of the sediment flux (also see Traykowski et al., this volume).

The flux estimates during the flood of January 1997 could only be accomplished by the indirect method, due to the lack of moored measurements in the plume. The results of these calculations are shown in Table 2. Using the rather uncertain estimates based on Eq. (5), approximately 20–60% of the sediment remained in the plume at the K-line during the peak flow measurements on December 31 and January 2. These proportions are similar to the 1998 observations, indicating that in both 1997 and 1998, more than half of the sediment discharged from the river was delivered to the bottom boundary layer to the south of the K-line.

Table 2
Sediment fluxes during flood of 1996–1997

	Q_f ($m^3 s^{-1}$)	C_{river} ($mg l^{-1}$)	Riverine flux (10^6 tons day^{-1})	K-line flux (10^6 tons day^{-1})	Fraction transported past K-line	Loss south of K-line (10^6 tons day^{-1})
31 Dec 1996	10,000	6000[a]	5	2.3	0.5	3
		15,000[b]	13		0.2	11
2 Jan 1997	9000	5000[a]	4	2.3	0.6	2
		13,000[b]	10		0.2	8
3 Jan 1997 a.m.	3500	3800[c]	1	0[d]	0[d]	1
3 Jan 1997 p.m.	3000	1300[a]	0.3	0[d]	0[d]	0.3
		3000[b]	0.8			0.8

[a] Concentration at mouth based on rating curve estimate ($C_{river} = \alpha Q_f^{\beta}$, $\alpha = 0.14, \beta = 1.139$).
[b] Concentration at mouth based on rating curve estimate ($C_{river} = \alpha Q_f^{\beta}, \alpha = 0.347, \beta = 1.139$).
[c] Concentration at mouth from bottle sample at 2-m depth.
[d] Flux is actually negative, due to wind reversal, but not significantly different from zero.

4.3.3. The influence of settling velocity

The analysis by Hill et al. (this volume) of floc distributions and settling rates in the plume, as well as prior measurements of flocs on the Eel shelf by Sternberg et al. (1999) suggest that there are two main populations of suspended sediment on the Eel shelf, a floc fraction with a mean settling velocity of around $1\,mm\,s^{-1}$, and a disaggregated fraction with a mean settling velocity of $0.1\,mm\,s^{-1}$ or less. A calculation was performed to determine how the velocity within and beneath the plume would affect the distribution of these two size classes of sediment, given the temporal variations of supply of sediment and the variations of velocity. The vertical trajectory of sediment was assumed to be dependent only on its settling velocity. This calculation was directed at the settling of sediment through the water column above the boundary layer, where resuspension and vertical turbulent fluxes could be neglected. The horizontal position was assumed to be controlled by an advection velocity, equal to the velocity measured as a function of depth at K-20. At positions offshore of the 20 m isobath, the velocity profile was assumed to be the same within the plume and to scale proportionately with depth below the plume. The sediment flux was assumed to be distributed evenly between the shore and the 40-m isobath, and to be negligible further offshore, approximating the observations. The amount of sediment delivered by the river was assumed to follow the same rating curve as the previous sediment flux calculations. An integration was performed between January 10 and 20, the period of high river discharge for which the ADCP data were available.

The results of this calculation (Fig. 12) indicate that the fast-settling particles arrive at the bottom boundary layer close to the river mouth, whereas the slow-settling particles are carried 20–60 km northward before reaching the bottom boundary layer. The difference is due to the difference in residence times of the particles: the typical residence time of a floc (settling velocity of $1\,mm\,s^{-1}$) is approximately 5.5 h, whereas the residence time of a disaggregated grain is 55 h. The

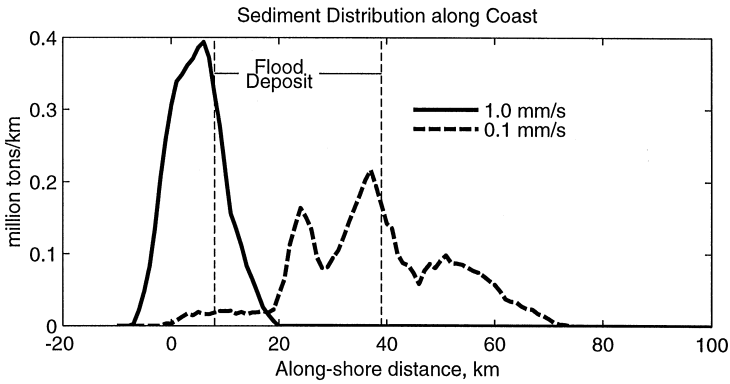

Fig. 12. Calculated estimates of the along-shelf distribution of sediment of sediment delivered from the Eel River between January 10 and January 20, 1998, assuming settling velocities of 1 mm s^{-1} (solid line) and 0.1 mm s^{-1} (dashed line).

peaks that occur at different locations along the shelf reflect the contributions of individual flood events and the details of the flow immediately following each event.

The above calculations of flux past the K-line indicate that 30–40% of the sediment is carried more than 10-km north of the mouth. This calculation indicates that most of the sediment that is transported that far is disaggregated, and that the fraction that is trapped to the south represents the floc fraction. The settling of 60–70% of the sediment to the south of the K-line could be explained if approximately that fraction of sediment is flocculated within the plume.

4.3.4. Delivery of sediment to the flood deposit

Wheatcroft et al. (1997) determined that the flood deposit from the 1995 flood lies between the 50- and 90-m isobaths. The 1997 flood produced a similar distribution of sediment deposition, with an integrated mass of approximately 7 million metric tons (Wheatcroft and Borgeld, this volume). These observations indicate that of about 21 million tons delivered from the river in 1997, 13 million tons fell out of the plume to the south of the K-line and 8 million tons were transported in the plume to the north. However, a negligible fraction was transported offshore, beyond the 50-m isobath, within the plume. Thus, the sediment transport by the plume clearly did not deliver the sediment to the flood deposit.

In spite of the large mass of riverine sediment delivered to the inner shelf, sedimentological data indicate that there is little mud deposition on the inner shelf, based on sediment grain size analysis (Wheatcroft and Borgeld, this volume). This suggests that either resuspension within the bottom boundary layer prevented sediment from settling, or that resuspension following the discharge events remobilized the sediment to be deposited elsewhere. There was substantial resuspension observed over the inner shelf (Figs. 7 and 8) following major floods, undoubtedly of fine sediment based on the vertical distribution of sediment and the intensity of the OBS signal. The near-bottom concentrations were not high enough

on January 15 to account for the sediment that had been trapped there, so a major fraction must have settled (unless it was rapidly transported seaward in the bottom boundary layer; see Traykovski et al., this volume). Thus, it appears that the sediment formed an ephemeral deposit on the inner shelf before being transported to the flood deposit and elsewhere (cf, Wheatcroft and Borgeld, this volume).

Intense bottom resuspension on the inner shelf due to wave orbital motions is more than adequate to remobilize this temporary inner shelf mud layer (Harris, 1999; Traykowski et al., this volume). Once remobilized, the sediment may have been transported offshore within the bottom boundary layer, driven by the excess density of a layer of fluid mud (Traykowski et al., this volume). According to the rough mass balance presented here, approximately half of the mass of sediment that fell out of the plume to the south of the K-line could account for the sediment that accumulated in the offshore flood deposit. The remainder of the sediment may have been dispersed in the seaward direction or transported along the coast. Observations by Alexander and Simoneau (1999) of sediment deposition on the continental slope to the north of the flood deposit suggest that there is widespread northward dispersal of Eel River sediment. The Eel Canyon to the south may be an offshore conduit for Eel River sediment as well, based on recent observations by Mullenbach and Nittrouer (personal communication, 1999).

5. Conclusions

Large floods of the Eel River produce a narrow, energetic plume that transports fresh water and sediment rapidly to the north over the inner shelf. The trajectory and speed of the plume are due both to the direct influence of the momentum and buoyancy of the outflow and the forcing by southerly winds. The nearly along-shelf orientation of the mouth of the river causes the momentum of the river outflow to be directed primarily along-shelf, which provides an important source of momentum to the plume and limits its offshore extent. Periods of high discharge are correlated with southerly winds, due to the association of low-pressure systems with high precipitation in the watershed. Strong southerly winds produce downwelling-favorable conditions over the shelf, augmenting the northward velocity of the plume and further narrowing of the plume. Tides perturb the along-shelf transport and possibly cause mixing at the mouth of Humboldt Bay, but they do not significantly alter the net transport of the plume. The plume is thin (5–7 m vertically), even during strong winds, attesting to the stabilizing influence of the large buoyancy flux.

The sediment transport by the plume is strongly dependent on plume speed and the settling rate of the suspended particles. During strong southerly wind conditions, the plume carries unaggregated, slowly settling particles more than 60-km north of the river mouth, whereas coarser grains and flocculated particles fall to the bottom boundary layer within 1-10-km of the mouth. During relatively infrequent occurrences of northerly winds, the plume slows down, and even the fine sediment settles close to the mouth. There is no significant offshore transport of sediment by the plume during either northerly or southerly winds, thus the plume does not

provide the offshore transport of sediment required to reach the mid-shelf flood deposit. Rather, the plume delivers the sediment to the bottom boundary layer on the inner shelf, possibly leading to the formation of an ephemeral mud deposit. Thus the seaward transport of sediment into the mid-shelf flood deposits and off the shelf must occur due to processes within the bottom boundary layer, including wave-induced resuspension and possibly the gravity-driven transport of dense suspensions (Traykowski et al., this volume; Ogston et al., this volume).

Acknowledgements

The authors thank Debbie Mondeel for coordinating the rapid response study, and the US Coast Guard Group Humboldt Bay for performing flights on short notice and in extreme weather conditions. Thanks to J. Lynch and J. Irish for implementation of the moored measurements. This work was supported by ONR's STRATAFORM program, grant #N00014-97-10134. Woods Hole Oceanographic Inst. contribution number 10005.

References

Alexander, C.R., Simoneau, A.M., 1999. Spatial variability in sedimentary processes on the Eel continental slope. Marine Geology 154, 243–254.

Allen, J.S., 1980. Models of wind-driven currents on the continental shelf. Annual Reviews of Fluid Mechanics 12, 289–433.

Armi, L., 1986. The hydraulics of two flowing layers with different densities. Journal of Fluid Mechanics 163, 27–58.

Borgeld, J.C., Hughes Clark, J.E., Goff, J.A., Mayer, L.A., Curtis, J.A., 1999. Acoustic backscatter of the 1995 flood deposit on the Eel shelf. Marine Geology 154, 197–210.

Brown, W.M., Ritter, J.R., 1971. Sediment transport and turbidity in the Eel River basin, California. US Geological Survey Water-Supply Paper 1986, 70pp.

Chao, S.-Y., Boicourt, W.C., 1986. The onset of estuarine plumes. Journal of Physical Oceanography 16, 2137–2149.

Chao, S.-Y., 1988a. River-forced estuarine plumes. Journal of Physical Oceanography 18, 72–88.

Chao, S.-Y., 1988b. Wind-driven motion of estuarine plumes. Journal of Physical Oceanography 18, 1144–1166.

Fong, D.A., 1998. Dynamics of freshwater plumes: observations and numerical modeling of the wind-forced response and alongshore freshwater transport. Ph. D. Thesis, MIT/WHOI, 98-16, 172 pp, in press.

Garvine, R.W., 1982. A steady state model for buoyant surface plume hydrodynamics in coastal waters. Tellus 34, 293–306.

Garvine, R.W., 1987. Estuary plumes and fronts in shelf waters: a layer model. Journal of Physical Oceanography 17, 1877–1896.

Garvine, R.W., 1995. A dynamical system of classifying buoyant coastal discharges. Continental Shelf Research 15, 1585–1596.

Geyer, W.R., Beardsley, R.C., Candela, J., Lentz, S.J., Limeburner, R., Johns, W.E., Castro, B.M., Soares, I.D., 1996. Physical oceanography of the Amazon Shelf. Contintental Shelf Research 16, 575–616.

Largier, J.L., Magnell, B.A., Winant, C.D., 1993. Subtidal circulation over the northern California shelf. Journal of Geophysical Research 98 (18), 147–18, 179.

Harris, C.K., 1999. The importance of advection and flux divergence in the transport and redistribution of continental shelf sediment. Ph.D. Thesis, University of Virginia Department of Environmental Sciences, 155pp.

Hill, P.S., Milligan, T.G., Geyer, W.R. Controls on effective settling velocity of suspended sediment in the Eel River flood plume. Continental Shelf Research 20, 2095–2111.

Kineke, G.C., Sternberg, R.W., 1992. Measurements of high concentration suspended sediments using the Optical Backscatterance Sensor. Marine Geology 198, 253–258.

Kudrayavtsev, V.N., Soloviev, A.V., 1990. Slippery near-surface layer of the ocean arising due to daytime solar heating. Journal of Physical Oceanography 20, 617–627.

Lentz, S.J., Winant, C.D., 1986. Subinertial currents on the southern California shelf. Journal of Physical Oceanography 16, 1737–1750.

Lentz, S.J., Limeburner, R., 1995. The amazon River plume during AmasSeds: spatial characteristics and salinity variability. Journal of Geophysical Research 100, 2355–2375.

Lentz, S., Guza, R.T., Elgar, S., Feddersen, F., Herbers, T.H.C., 1999. Momentum balances on the North Carolina inner shelf. Journal of Geophysical Research 104, 18,205–18,226.

Milligan, T.G., Krank, K., 1991. Electro-resistance particle size analyzers. In: Syviski, J.P.M. (Ed.), Principles, Methods and Applications of Particle Size Analysis. Cambridge University Press, New York, pp. 109–118.

Milliman, J.D., Syvitski, J.P.M., 1992. Geomorphic/tectonic control of sediment discharge to the ocean: the importance of small mountainous rivers. Journal of Geology 91, 1–21.

Morehead, M.D., Syvitski, J.P., 1999. River-plume sedimentation modeling for sequence stratigraphy: application to the Eel margin, northern California. Marine Geology 154, 29–42.

Nash, D.B., 1994. Effective sediment-transporting discharge from magnitude-frequency analysis. Journal of Geology 102, 79–95.

Ogston, A., Cacchione, D.A., Sternberg, R.W., Kineke, G.C. Observations of storm and river flood-driven sediment transport on the Northern California continental shelf. Continental Shelf Research 20, 2141–2162.

Rennie, S.E., Largier, J.L., Lentz, S.J., 1999. Observations of a pulsed buoyancy current downstream of Chesapeake Bay. Journal of Geophysical Research 104, 18,227–18,240.

Sommerfield, C.K., Nittrouer, C.A., 1999. Modern accumulation rates and a sediment budget for the Eel shelf: a flood dominated depositional environment. Marine Geology 154, 227–242.

Sternberg, R.W., Berhane, I., Ogston, A.S., 1999. Measurement of size and settling velocity of suspended aggregates on the northern California continental shelf. Marine Geology 154, 43–54.

Syvitski, J.P., Morehead, M.D., 1999. Estimating river-sediment discharge to the ocean: application to the Eel margin, northern California. Marine Geology 154, 13–28.

Traykovski, P., Geyer, W.R., Irish, J.D., Lynch J.F. The role of wave-induced density-driven fluid mud flows for cross-shelf transport on the Eel River continental shelf. Continental Shelf Research 20, 2113–2140.

Wheatcroft, R.A., Sommerfield, C.K., Drake, D.E., Borgeld, J.C., Nittrouer, C.A., 1997. Rapid and widespread dispersal of flood sediment on the northern California margin. Geology 25, 163–166.

Wheatcroft, R.A., Borgeld, J.C. Oceanic flood deposits on the northern California shelf: large scale distribution and small-scale physical properties. Continental Shelf Research 20, 2163–2190.

Yankovsky, A.E., Chapman, D.C., 1997. A simple theory for the fate of buoyant coastal discharges. Journal of Physical Oceanography 27, 1386–1401.